Engineering Structures 308 (2024) 117966

Contents lists available at ScienceDirect

Engineering Structures

journal homepage: www.elsevier.com/locate/engstruct

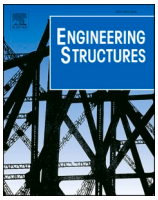

Shear tests on full-scale bridge slabs with bent-up reinforcing bars

Tobias Huber [a,*,1,2], Patrick Huber [a], Hannes Wolfger [a], Markus Vill [b], Johann Kollegger [a]

[a] Institute for Structural Engineering, Vienna University of Technology, Karlsplatz 13/212-2, 1040 Vienna, Austria
[b] FH Campus Wien – University of Applied Sciences, 1100 Vienna, Austria

ARTICLE INFO

Keywords:
Shear strength
Full-scale testing
Bent-up bars
Concentrated load

ABSTRACT

Shear reinforcement design has changed over time, along with the knowledge about the shear behaviour of reinforced concrete structures. Until the 1970s, the shear design in Europe was based on empirical limits for shear stress. The rules stipulated by the design standards often resulted in designs of concrete slabs with shear reinforcement consisting only of bent-up bars without any additional stirrups. Today, truss models are widely used to design shear reinforcement. However, in the structural assessment of bridges with bent-up bars, it is difficult to apply such models due to their specific detailing requirements. In order to evaluate the applicability of current design standards and to span the knowledge gap between the load-bearing behaviour of small-size specimens and actual structures, four shear tests on two full-scale replica bridge slabs containing bent-up bars are presented in this paper. The applied load configuration represents two-axle and four-wheel loads of the current load models for railway bridges stipulated by Eurocode 1–2 and train load model UIC 71. The load distribution due to a track superstructure consisting of a track, sleepers and ballast was investigated. A comparison of the obtained results with those of preliminary tests on narrow slab strips shows differences in the load-bearing behaviour of small-format laboratory tests. The results of the analysis of the bridge slabs according to various design standards show the potential of the newly developed potential shear crack model for the assessment of slab bridges with bent-up reinforcing bars.

1. Introduction

Since many structures built in the last century have reached, or will soon reach, the end of their theoretical service life, the following question arises: can we continue using these structures? In order to guarantee safe use, the structures must exhibit sufficient load-bearing capacity according to the semi-probabilistic security concept stipulated in current design standards. In Germany, rigorous structural assessment of road bridges has been conducted which showed that around 50% of 143 bridges exhibit a lack of shear capacity [1]. Among these, a third of 27 analysed slab bridges were found wanting due to insufficient shear reinforcement and detailing issues. Results like these gave rise to the development of refined shear models all over Europe. The goal of these models is to adequately model the shear behaviour of such bridges [2], especially those with reinforcement designs from the past that are no longer covered in current standards, such as bent-up bars used as shear reinforcement [3]. Bent-up bars were commonly used until the 1970s; however, they are less common nowadays due to the complicated process of bending of bars with large diameters and placing such reinforcement on site. Also, the occurrence of larger shear crack widths under service load due to the large diameters of the bent-up bars led to the transition to stirrups as the preferred type of shear reinforcement [4].

In the early days of reinforced concrete construction, Mörsch [5] developed a graphical procedure to determine the required number and positions of bent-up bars based on the acting shear stress $\tau = V/b{\cdot}z$ (Fig. 1a,b). Until the 1970s, however, the procedure was rarely used since the empirically derived limits for shear stress stipulated in the Austrian and German design standards [6,7] were much higher than those found in subsequent standards [8,9]. If these limits were not exceeded, the only detailing rule was that longitudinal bars had to be bent upwards if not needed to cover the bending moments (Fig. 1c). From the 1970s onward, it became more common to use the graphical procedure due to lower shear stress limits [10,11] (Fig. 1b,c). Some approaches assumed the concrete to transfer a portion of the shear stress (Fig. 1a), while in others the reinforcement was assumed to transfer the entire shear stress (Fig. 1b). Bent-up bar layouts designed according to

* Corresponding author.
E-mail address: tobias.alexander.huber@tuwien.ac.at (T. Huber).
[1] ORCID: 0000-0001-9248-1662.
[2] URL: http://www.betonbau.tuwien.ac.at

https://doi.org/10.1016/j.engstruct.2024.117966
Received 12 February 2024; Accepted 31 March 2024
Available online 17 April 2024

Nomenclature

Ø	Bar diameter
A_s	Cross-section area of the reinforcement
A_0	Support force due to the self-weights of the slab and the superstructure
A_F	Support force due to external load
C	Bedding modulus
E	Young's modulus
F	Force; point load
L	Elastic length
M	Bending moment
V	Shear force
V_C	Shear resistance attributed to the concrete
V_F	Shear force due to external load
V_{Exp}	Maximum shear strength in the experiment
V_S	Shear resistance attributed to the transverse reinforcement
a	Shear span (distance between support and point load)
b	Width
c	Compression zone depth; cement
d	Static depth of the beam
d_g	Maximum size of aggregate
f_c	Concrete cylinder compressive strength
f_{ct}	Tensile strength of the concrete
f_t	Tensile strength of the reinforcing bar
f_y	Yield strength of the reinforcing bar
g	Dead load due to the self-weights of the slab and the superstructure
h	Height of the structural member
k	Stiffness
l	Length
m	Mean value
s_b	Horizontal spacing between bent-up bars
s_a	Horizontal spacing between the edge of the support and the theoretical bending point of the first bent-up bar
z	Inner lever arm
α	Angle of the inclined portion of the bent-up bar
β	Idealised crack angle
δ	Relative deflection
ε_s	Reinforcement strain
ρ	Longitudinal reinforcement ratio
ρ_w	Shear reinforcement ratio
$\rho_{w,min}$	Minimum shear reinforcement ratio according to structural standards
τ	Shear stress
θ	Truss angle or angle of the stress field
Δ	Height extension
DIC	Digital image correlation
LVDT	Linear variable differential transformer
RC	Reinforced concrete
SG	Strain gauge

either type of approach are difficult to assess with current standards, as will be shown more in detail in Section 4 (due to, e.g., wide spacings between groups of bent-up longitudinal bars, a single group of parallel bent-up bars etc.). In addition, the standards also allowed the use of truss model approaches (Fig. 1d), but their application was required only if certain shear stress limits were exceeded. It is important to note that most of the bridges designed to these standards do not show any signs of shear problems in inspections (e.g., pronounced shear cracking or deformation).

In addition to current shear models not being suitable to be used on bridges with old shear reinforcement layouts, these models were all calibrated on databases containing only results of small-scale tests under point loads. Furthermore, the database of tests with ribbed bent-up bars is somewhat limited [4,12–14]. Thus, full-scale testing of decommissioned bridges could be a promising approach for investigating the load-bearing behaviour of past reinforcement designs. A comprehensive review of full-scale bridge tests has been carried out by Bagge [15], yielding a database of 30 bridges tested to failure. Only six of these bridges were reinforced concrete slab bridges which failed in shear. Evaluating whether the actual reinforcement of slab structures matches

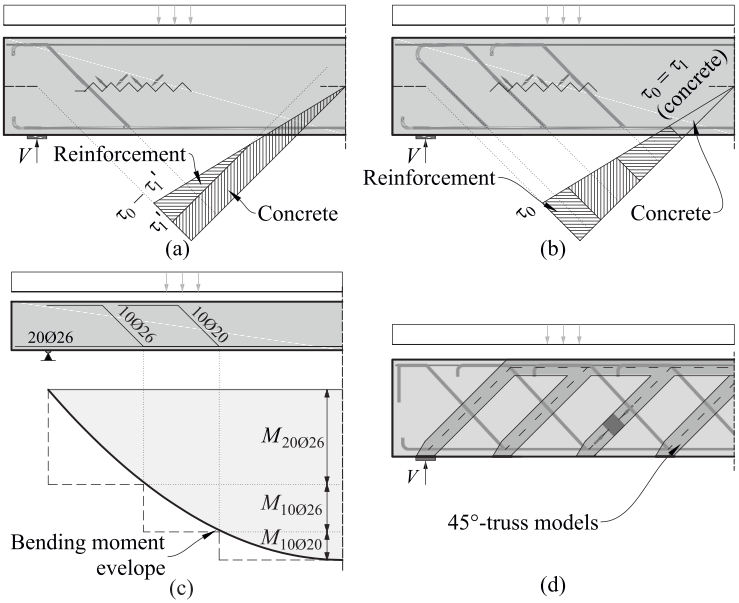

Fig. 1. Principle of shear design with bent-up bars: according to principal tensile stresses (a) with and (b) without assuming shear to be transferred by the concrete; (c) according to the bending moment envelope; (d) according to truss models.

the design drawings and retrieving mechanical parameters representative of the entire structure are complex tasks. Moreover, the influence of deterioration on the structural capacity of an as-built structure several years after construction has to be taken into account but is difficult to assess. In the present study, the task is approached differently: by testing replicas of a representative bridge slab, thus possessing reliable data of the reinforcement layout and all mechanical parameters. Furthermore, a realistic testing concept was used to identify any capacity reserves (Fig. 2).

In this paper, the results of four shear tests on two full-scale replica bridge slabs are presented. The slabs were loaded with a realistic load configuration representing two-axle and four-wheel loads of the loading model for railway bridges according to Eurocode 1–2 and train load model UIC71. The load distribution due to the track superstructure consisting of a track, sleepers and ballast and its influence on the shear capacity are investigated. Furthermore, the influence of the slab width on the shear capacity is investigated by comparing the results with those of preliminary tests on slab strips with a tenth of the slab width (reported in [16]). The achieved experimental loads are compared with the results obtained from current models available in Eurocode 2, ACI318, fib MC2010 and from the potential shear crack model (PSCM) of the Austrian structural assessment standard ÖN B4008–2 [17]. Since the use of shear models of current standards requires many assumptions and undefined interpretations to be made, these are explained one by one.

2. Full-scale experiments

2.1. Specimens

Two test slabs with a height of 660 mm, a width of 3800 mm and a length of 9.0 m were tested (Fig. 3). The longitudinal reinforcement consisted of 38 longitudinal bars Ø26 and Ø20, spaced at 100 mm. The secondary reinforcement consisted of 60 bars Ø14, spaced at 150 mm. The concrete cover is 30 mm, which results in a static depth d of around 600 mm. In the middle of the span, the reinforcement ratio $\rho = A_s/(b{\cdot}d)$ is 0.80% (29Ø26 mm + 9Ø20 mm). A single group of parallel bent-up bars (10Ø26 mm) was placed at one end of the slab. They were spaced at s_a= 700 mm, which is the distance between the support and the theoretical intersection point between the bent-up bars' inclined portion and the longitudinal reinforcement axis. Thus, the reinforcement ratio decreases to 0.57% beyond the bends of the bent-up bars. At the other end of the slab, an additional group of parallel bent-up bars (9Ø20 mm) was placed at a distance s_b of 800 mm from the first group. Thus, the reinforcement ratio decreases to 0.68% and 0.47% after the first and second group of bars, respectively. The layout of the bent-up bars was designed according to technical drawings of existing Austrian railway bridges. It is important to note that the bridge slabs to be tested were initially 4000 mm wide, but the edges had been cut off on both sides (100 mm, see Fig. 3) to avoid any undue influence by the edge reinforcement (Fig. 2c,d) on the test results. The initial width was required for another investigation [18]. The specimens from preliminary tests on slab strips [16] are also shown in Fig. 3. The slab strips with a width of 400 mm have the same reinforcement configuration as the slabs.

The test parameters are reflected in the specimen names as listed in Table 1. The first two letters and accompanying number indicate the tested component (SL: slab, SS: slab strip; #1 or #2). An additional group of parallel bent-up bars is indicated by the letter z, and the presence of the full superstructure by the letter o. If a tandem load configuration was used, the letter t is added at the end.

2.2. Materials

To ensure comparability of the results, both the test slabs and the specimens of the preliminary tests were cast from the same batch of the ready-mixed concrete (C25/30; see Table 2). It should be noted that the slabs were cast and stored outdoors, while the strips were cast and stored inside the prefabrication plant. The air void content determined on site was 1.0%.

During the casting of the slabs, twelve cylinders (Ø = 150 mm, h = 300 mm) were also produced to determine the cylinder compressive strength f_{cm}, the splitting tensile strength $f_{ct,sp}$ and the Young's modulus E_{cm}. In addition, six cubes (h = 150 mm) were produced to determine the compressive strength $f_{cm,cube}$. The mean values of the material parameters were determined from three individual tests carried out 28 days

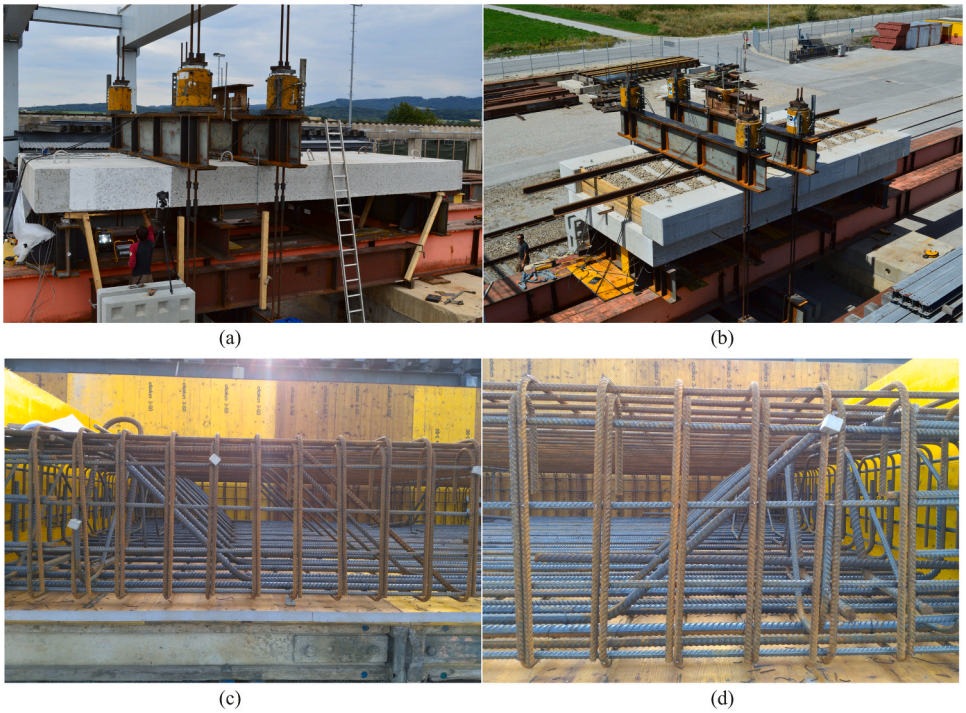

Fig. 2. Full-scale testing: (a) slab without superstructure, (b) slab with superstructure, (c) two rows of bent-up bars and (d) a single row of bent-up bars.

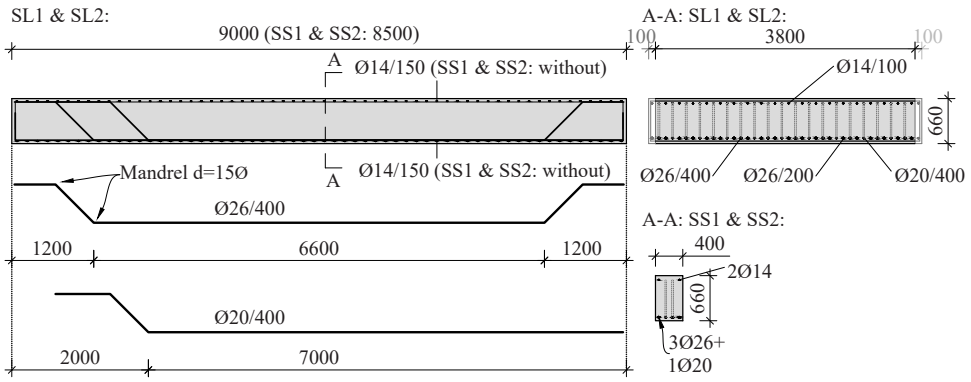

Fig. 3. Reinforcement layout of the tested slab and the slab strips from [16].

Table 1
Details of reinforcement and loading, mechanical properties of the concrete and experimentally determined shear strengths.

Specimen		Span (mm)	Width (mm)	g (kN/m)	Loads	Bent-up bars[a]	f_c (MPa)	f_{ct} (MPa)	A_0 (kN)	V_F (kN)	V_{Exp}[f] (kN)
SL1	SLz–t	8000	3800	62.7	3d & 5.67d	10Ø26 @ 700 9Ø20 @ 1500	52.1[e]	4.18	356.0	2656.2	2980.8[c]
	SL–t				3d & 5.67d	10Ø26 @ 700			358.6	2002.2	2329.5
SL2	SLzo–t			123.5	3d & 5.67d	10Ø26 @ 700 9Ø20 @ 1500			631.7	2630.5	3200.4[c]
	SLo–t				3d & 5.67d	10Ø26 @ 700			629.8	2055.2	2623.4
SS1	SSz–t	8000	400	6.6	3d & 5.67d	1Ø26 @ 700 1Ø20 @ 1500	39.7[e]	3.49	32.7[g]	255.5	284.9[c]
	SS				3d	1Ø26 @ 700			31.3[g]	295.8	323.8
SS2	SSz	6200[b]			3d	1Ø26 @ 700 1Ø20 @ 1500			25.4[g]	339.4	361.5[c]
	SS–t	8000			3d & 5.67d	1Ø26 @ 700			32.7[g]	254.8 231.0	284.2[c] 260.4[d]

[a] Distance to the centre of the support in mm.
[b] Span shortened due to damage from first test.
[c] Flexural failure.
[d] Shear failure after re-loading.
[e] calculated with (1)
[f] calculated with $V_{Exp} = V_F + A_0 - g \cdot a$ (for a see Fig. 12).
[g] Dead load calculated from nominal dimensions, assuming $\gamma = 25$ kN/m^3 for reinforced concrete.

Table 2
Concrete composition (amounts in kg/m^3).

	Class	m (kg/m^3)
Aggregate	0/4	912
	4/8	170
	8/16	377
	16/32	431
Cement	CEMII/42.5 N	270
Hydraulic additives		68
Water		173
Plasticiser	Visco 3088 VP	2
Total		2401

after casting and after execution of the shear tests (561 days after casting). The results are listed in Table 3.

The results show that pronounced hardening took place between days 28 and 561 (Table 3). The slab strips and slabs were tested 41 days and 440 to 469 days after casting, respectively. In order to estimate the concrete properties on the day of testing, the amount of hardening was calculated using time-dependent concrete properties according to EC2 (1):

$$f_{cm}(t) = \beta_{cc}(t) \cdot f_{cm} \text{ with } \beta_{cc}(t) = e^{s\left[1-\sqrt{28/t}\right]}, \quad (1)$$

where t is the age in days and s is a coefficient depending on the early strength development of the concrete.

The parameter $s = 0.47$ was determined from the test results. Subsequently, the strength on the testing days was calculated with Eq. (1); the values obtained are listed in Table 1. The material parameters of the longitudinal reinforcement were each determined in three tensile tests carried out by an external testing institution (Table 4). Ribbed bars of class B550B with diameters of Ø20 mm and Ø26 mm were used as the slab reinforcement.

Table 3
Mechanical properties of the concrete at different ages.

Age (days)	f_c (MPa)	$f_{c,cube}$ (MPa)	f_{ct} (MPa)	E_c (GPa)
28	36.6	46.1	3.05	29.602
	± 1.8%	± 2.5%	± 1.2%	± 0.2%
561	52.6	71.2	4.36	38.140
	± 4.3%	± 2.7%	± 2.4%	± 1.5%

Table 4
Mechanical properties of the reinforcing bars.

	Ø [mm]	$Ø_{meas}$ [mm]	f_y [N/mm^2]	f_t [N/mm^2]
SL1, SL2	20	19.9	556.2	670.5
	26	25.7	583.8	657.4
SS1, SS2	20	–	598.1	686.1
	26	–	563.4	656.4

2.3. Test setup

2.3.1. Direct loading of the bridge slab

The influence of the slab width on the shear strength was investigated in two shear tests on slab SL1 without superstructure and by comparing the results with those from tests reported in [16] (SS-t, SSz-t; Table 1). At the same time, two different bent-up bar layouts ($\alpha = 45°$) were investigated. The configuration of the bent-up bars and the load arrangement in the longitudinal direction ($a = 3.0{\cdot}d$ or $5.67{\cdot}d$) were the same as those in the preliminary tests on slab strips (Table 1, Fig. 3).

Fig. 4 shows the experimental setup for test SLz–t. In the second test, the positions of the loads were reversed with respect to the centre of the span. The loads were introduced on auxiliary beams HEB800 strengthened with two lamellae of 30 mm thickness which were loaded by four hollow piston jacks with a total capacity of 500 tons each (Type VSL ZPE500). The individual loads were applied at a distance of 1.6 m in the longitudinal direction and a distance of 1.5 m transversally. The area of load application was 0.09 m^2 (loading plate: 0.3 × 0.3 m). In the presented tests, the supports consisted of four individual bearing points on each side. The loaded end was equipped with a total of eight load cells. A steel plate (250 mm × 250 mm × 30 mm) and an elastomeric plate (250 mm × 250 mm × 40 mm) were placed on top of each pair of load cells. At the other, unloaded end, elastomeric bearings (200 mm × 250 mm × 70 mm) were placed on blocks of tubular steel (Ø250 mm, $h = 130$ mm). The load cells were moved to the opposite end after the first test (due to the reversed load positions).

2.3.2. Slab with superstructure

The second slab was built including a superstructure consisting of rails, sleepers and a 550 mm ballast bed (Fig. 5). The required edge beams were cast separately and each block (length 2.25 m, height 0.6 m) was mounted onto the slab using two formwork ties (Fig. 5a,b). The influence of this realistic superstructure on the shear resistance of slab SL2 was investigated by comparing the test results with those of slab SL1 (SL1-t, SL1z-t). The concrete mix, the configuration of the bent-up bars and the loading in the longitudinal direction ($a = 3.0d$ or $5.67d$) were identical for both slabs (Table 1). Fig. 5a shows the test setup for the second test on slab SLo–t. The first test was carried out with the load positions reversed with respect to the centre of the span. The loads were applied directly on the rails which were strengthened with rail brackets at the load application points (Fig. 5b). The geometric arrangement of the loads corresponds exactly to the load model 71 as described in [19].

2.4. Instrumentation

Fig. 4 shows the extensive measurement programme for the tests. The support forces (V_i) and resulting deflections (δ_i) were determined using conventional measurement devices such as load cells and inductive displacement transducers (LVDT; Fig. 4). The relative vertical displacements underneath both load introduction points were determined taking into account the deflections measured at the supports. In addition, the change in height (Δ_i) at four locations was monitored by LVDTs (Fig. 4). LVDTs and strain gauges were used to determine the principal strains (ε_i) at the concrete surface on the tension side (bottom) and compression side (top) of the slab, respectively. During the holding phases, oil pastels were used to trace the crack patterns. Additionally, a digital image correlation system (DIC) was utilised to detect cracks at the bottom of the slab.

2.5. Results

The load–deflection curves, vertical support force distribution and height monitoring results are shown in Fig. 6.

All diagrams in Fig. 6 show a comparison of the two tests performed on the same slab by displaying the results for both the slab ends with two rows of bent-up bars (red) and for that with a single row of bent-up bars (black). It is important to note that the self-weights of the slab and the superstructure are not considered in the forces or deflections displayed in these diagrams. The support forces induced by the dead load (V_0) were measured before testing and are listed in Table 1.

From the results, it can be concluded that the shear capacity increased by at least 33% by the presence of an additional row of bent-up bars (comparison of SLz-t with SL-t). The presence of the superstructure led to an increase in shear capacity of 13.7% (comparison of SLo-t with SL-t). Figs. 6a and 6d show the comparison of the load–deflection behaviours of tests SLo-t and SL-t. It should be noted

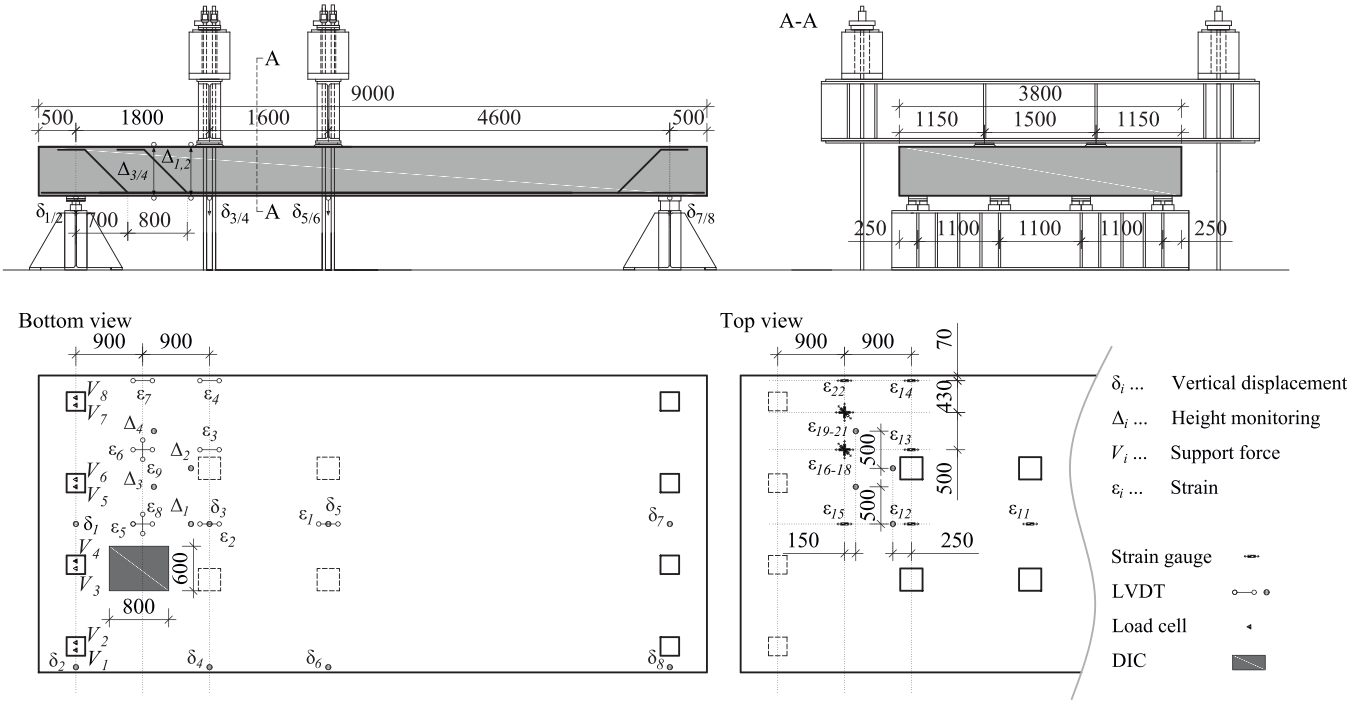

Fig. 4. Test setup for slab SL1 under directly applied loads, and instrumentation applied in all four tests.

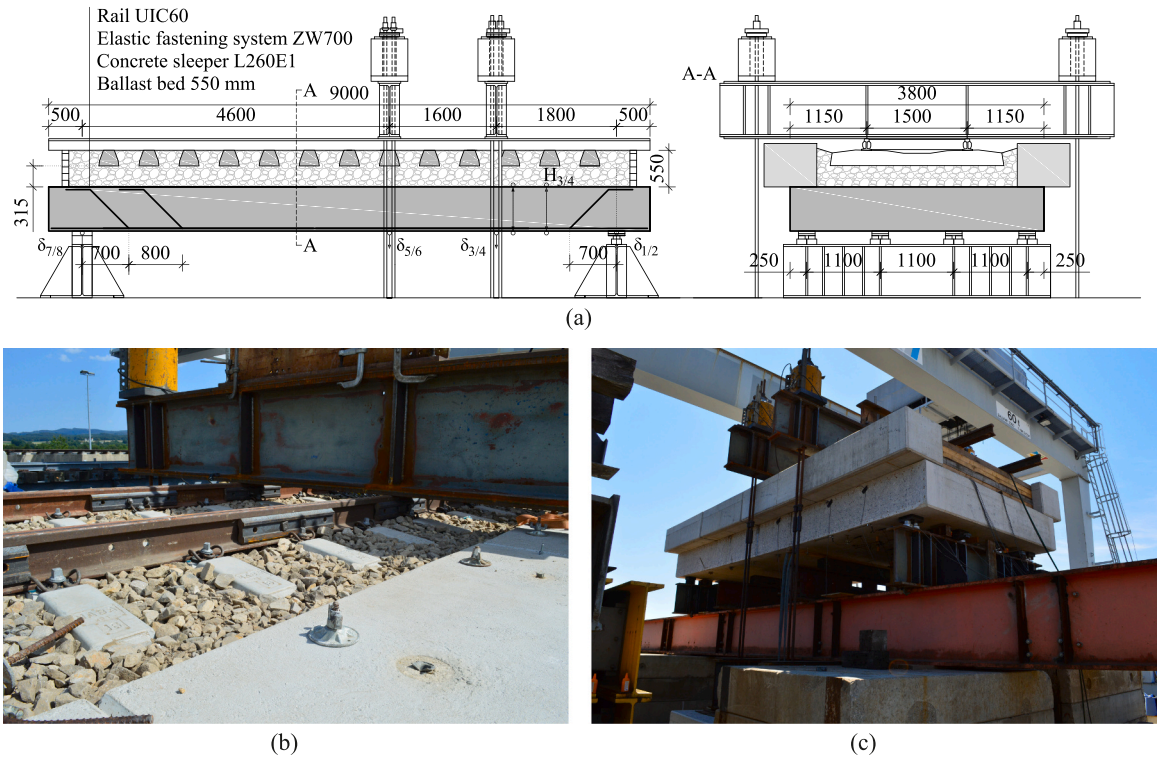

Fig. 5. Testing of the slab with superstructure: (a) load arrangement and layers of the superstructure; (b) reinforced load introduction point and mounted edge beam; (c) test setup.

that the deflections measured at the edge (δ_4, δ_6) and in the centre of the slab (δ_3, δ_5) were the same in all four tests. As can be seen in Figs. 6a and 6d, the initial stiffnesses were lower in the second tests since the slabs had gained flexural cracks over their entire lengths in the first tests (see black cracks in Fig. 7). The change in stiffness was more pronounced in the slab with superstructure (Fig. 6d) as the slab had been fully uncracked before testing, whereas the slab without superstructure had been loaded before the ultimate load test [18]. The slab ends with a single row of bent-up bars (SL–t and SLo–t) failed in shear, exhibiting a sudden increase in deflection. The slab ends containing two rows of bent-up bars (SLz–t and SLzo–t) exhibited flexural failure, with yielding plateaus in the associated load–deflection curves just before the loading procedure was aborted (Fig. 6a,d). The post-failure crack patterns with photos of examples are displayed in Fig. 7.

Both shear failures were characterised by failure along an inclined flexural shear crack in the region without shear reinforcement (Fig. 7b, e). The flexural failures were characterised by a single pronounced vertical crack located at the second load introduction point (Fig. 7a,d). Fig. 7 shows the flexural cracks which tended to propagate along the secondary reinforcement (spaced at 150 mm), with every other crack being more pronounced (see side views of the slabs in Fig. 7). Interconnections of those cracks within the testing area were found at the bottom of the slabs (Fig. 7). The slab without superstructure exhibited cracks at various angles at the top, including punching cracks in the area around the loading plate (Fig. 7c), whereas in the other slab there were almost no cracks visible after removal of the superstructure. It should be noted that the observed punching cracks do not indicate shear punching but rather result from the critical shear crack having propagated to the second load introduction point. The principal strain directions were calculated from the strain gauge measurements and are displayed in Fig. 7 for load V_F. It should be noted that the principal directions remained almost constant for loads $V > 0.5 \cdot V_F$. The calculated directions correspond to the actual orientations of the cracks, as can be seen in Fig. 7.

Figs. 6b and 6e show the deviation of the individual vertical support forces from an average support force that assumes equal load distribution to all four bearing points. As expected, the load tends to be distributed towards the inner supports, with a 7% higher load than the average, whereas the outer supports bear a 7% lower load. In all tests, it was observed that one of the inner bearings was loaded more than the other (Fig. 6, Table 5).

In the tests with shear failures (shown in black in Fig. 6), a redistribution of forces towards one side occurred after V_F had been reached, as shown in Figs. 6b and 6e.

Figs. 6c and 6f show the results of the height monitoring performed at several points in the testing area (Fig. 4). The measurements of the tests with a single row of bent-up bars (SL–t, SLo–t) show increasing rates of height extension starting around a load of $V = 1750$ kN, compared to results from specimens with two rows of bent-up bars (SLz–t, Slzo–t). After reaching the peak load (V_F), with values of $\Delta_{3/4}$ between 0.4–0.6 mm, the height extension increased to 1.65 mm in the test without superstructure (SLz–t) and to 3.81 mm in the test with superstructure (SLzo–t) before the slab collapsed. A comparison of the values obtained at the same longitudinal positions (Δ_3 and Δ_4; Δ_1 and Δ_2) leads to the conclusion that the shear crack opened in equal amounts over the entire width of the slab.

3. Discussion of the test results

3.1. Influence of the track superstructure on the stress resultants

In laboratory tests, loads are typically applied directly to the test specimens, while in reality, the loads are usually distributed by the railway superstructure. As no measurements of the pressure under the ballast were performed (see Section 2.4), several models for load distribution are evaluated in the following. Eurocode 1 [19] provides approaches for the distribution of point loads within the load models for roads and railways for design. For railways, the point loads of Load Model 71 may be distributed uniformly in the longitudinal direction if ballast is provided. Assuming an equal distribution for the tests with

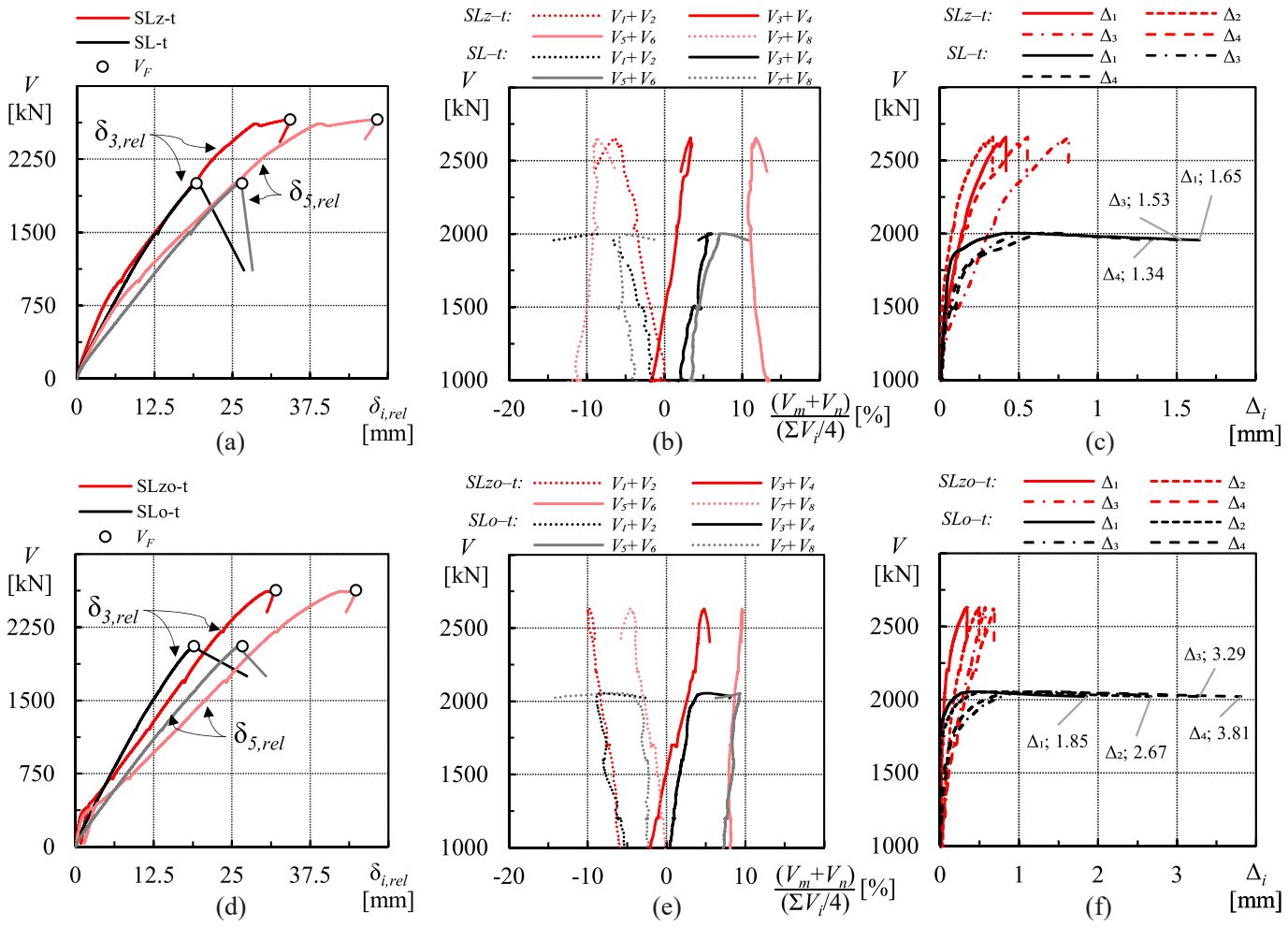

Fig. 6. Results for tests without superstructure: (a) load–deflection diagram; (b) deviation of the individual vertical support forces from the mean of the support forces; (c) height monitoring. Results for the tests with full superstructure: (d) load–deflection diagram; (e) deviation of the individual vertical support forces from the mean of the support forces; (f) height extension monitoring.

superstructure, the resulting load distribution length $l_d = 3.20$ m is two times the distance between the point loads of train load model UIC71. Furthermore, each point load can be distributed longitudinally over three sleepers should local load effects be of relevance, while a constant distribution over the whole sleeper width is assumed in the transverse direction. Within the ballast, a gradient of distribution of 4:1 can be assumed (Fig. 8c). Applying the principles for local load effects mentioned above on the conducted test setup yields a load distribution length of $l_d = 2.86$ m (see Fig. 8d).

A more refined approach is the model of a beam on elastic foundation [20,21]. The model is usually used to calculate the bending stresses of rails under the basic assumption that the deflection of the rail is proportional to that of the foundation. Zimmermann [21] provides the concept of an idealised longitudinal beam (rail and sleepers) resting on an elastic foundation (Fig. 8a). It can be shown that the stress resultants of the idealised longitudinal beam are identical to those of a stiff beam of twice the elastic length L [19]. The width b_l of the idealised beam is calculated as:

$$b_l = l_a \cdot \frac{b_s}{a} = 1.05 \cdot \frac{0.30}{0.60} = 0.525 \text{ m}, \tag{2}$$

where l_a is the load distribution length in the transverse direction, assuming a load-free strip of 0.50 m in the centre to take into account rail compaction [21], b_s is the width of sleeper L260E1 and a is the spacing of the sleepers.

The elastic length L is then calculated as:

$$L = \sqrt[4]{\frac{4 \cdot E_R \cdot I_R}{C \cdot b_l}} = \sqrt[4]{\frac{4 \cdot 2.1 \cdot 10^5 \cdot 3.0383 \cdot 10^{-5}}{C \cdot 0.525}}, \tag{3}$$

where E_r is the Young's Modulus of rail UIC60E1, I_r is the moment of inertia of the rail, C is the bedding modulus of the foundation underneath the idealised beam and b_l is width of the idealised beam.

In the conducted tests, an elastic fastening system produced by Getzner Werkstoffe GmbH was used, with the stiffness retrieved from datasheets of compression tests with magnitudes ranging between 16–68 kN. The bedding modulus of the other layers is usually difficult to determine since this parameter is load-dependent and strongly depends on the ground conditions. Table 6 lists approximate values found in literature.

Nevertheless, it is possible to determine the actual stiffness since the relative deflection of the slab was measured at locations beyond the load introduction points. As shown in Fig. 6d (SLzo–t), the stiffness remains rather constant after initiation of cracking. For $V = 2000$ kN ($F/2 = 1482$ kN), stiffness values of 52 MN/m and 72 MN/m were determined for the locations of δ_3 and δ_5, respectively. As for the ballast, a Young's modulus of $E = 150$ MN/m^2 can be assumed which is rather stiff compared to the other layers. For the sake of simplicity, this layer is not considered in the analysis. Table 7 shows the compositions and stiffnesses of the layers. It should be noted that there were no other elastic layers such as sleeper pads or ballast matting (Table 7).

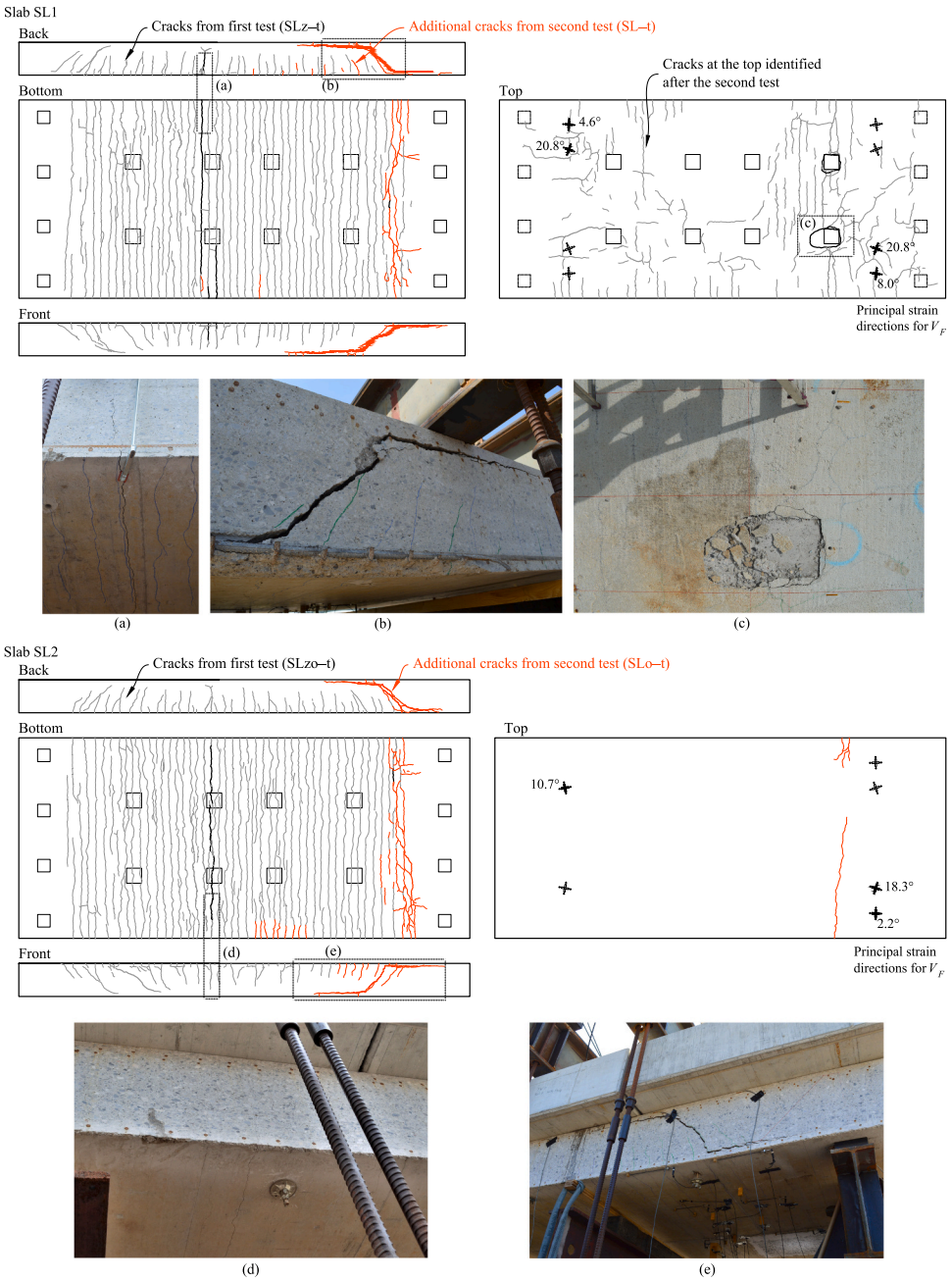

Fig. 7. Principal strain directions at the top for load V_F and post-failure cracking pattern displayed for the first (black) and second test (red): (a) critical flexural crack of specimen SLz–t; (b) critical shear crack and (c) punch-through of the loading plate of specimen SL–t; (d) critical flexural crack of specimen SLzo–t; (e) critical shear crack of specimen SLo–t.

Table 5
Vertical support forces for V_F.

Specimen		V_{1+2} [kN]	V_{3+4} [kN]	V_{5+6} [kN]	V_{7+8} [kN]	V_F [kN]
SL1	SLz–t	621.9 (−6.3%)	686.5 (+3.4%)	742.1 (+11.8%)	605.6 (−8.8%)	2656.2
	SL–t	463.2 (−7.5%)	530.7 (+6.0%)	538.1 (+7.5%)	470.3 (−6.0%)	2002.2
SL2	SLzo–t	593.5 (−9.7%)	689.1 (+4.8%)	720.5 (+9.6%)	627.5 (−4.6%)	2630.5
	SLo–t	472.3 (−8.1%)	540.6 (+5.2%)	561.7 (+9.3%)	480.6 (−6.5%)	2055.2

The stiffness of the entire system shown in Table 7 is used to calculate the bedding modulus $C = k/(b_l \cdot a)$ in Eq. (3). The resulting elastic lengths L are 0.86 m and 0.82 m for the locations of δ_3 and δ_5, respectively. By following the same logic, an averaged elastic length (L = 0.84 m) is assumed and a load distribution length l_d = 3.28 m is determined for the test configuration (Fig. 8b). If the lower limit for the bedding modulus for bridges of 300 MN/m^2 (see Table 6) were used, the elastic length would be L= 0.80 m, which agrees well with the analysis above. Additionally, if the contribution of the elastic fastening system were omitted, the elastic length would be L = 0.63 m. This confirms the distribution of the load over three sleepers, as suggested by Eurocode 1.

Fig. 9 shows the calculated stress resultants for a beam at load V_{Exp}. The calculation of the stress resultants considers the distribution length l_d = 3.28 m as well as the dead load. Formulas are given in Appendix A.

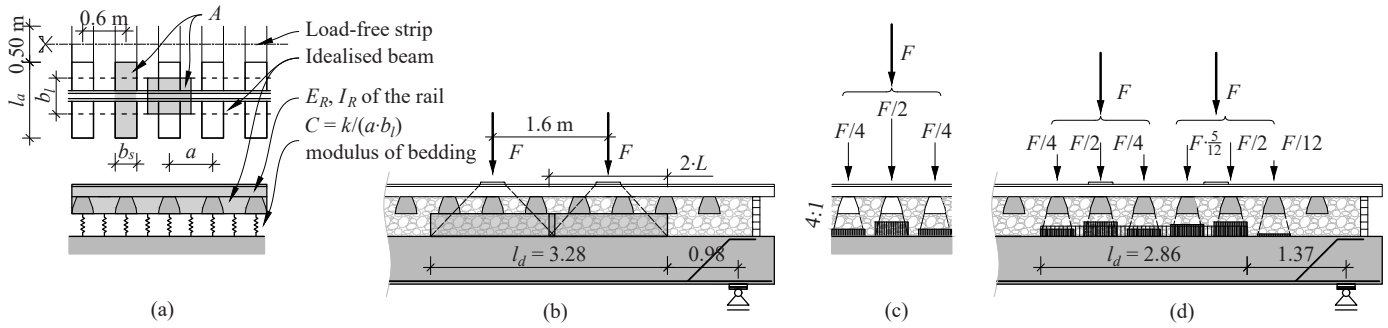

Fig. 8. Load distribution in the longitudinal direction: (a) beam on elastic foundation according to Zimmermann [21]; (b) load distribution over three sleepers according to Eurocode 1 [19]; (c) application of [21] for tests with superstructure; (d) load distribution over three sleepers [19] for tests with superstructure.

Table 6
Dependence of the bedding modulus on the ground conditions [22,23].

Ground conditions	Bedding modulus [MN/m³]
Poor (water-saturated soil, narrow graded sands)	20
Bad (cohesive soil)	50
Good (gravel)	100–150
Very good (concrete, bridges, tunnels)	300–600

Table 7
Layer compositions and stiffnesses.

Layer	Type	Stiffness [MN/m]	
Elastic fastening system	ZW 700b/60	k_{Fs}	60
Sleeper	L260E1		stiff
Sleeper pads	none		–
Ballast	GK 31.5/63 h = 310 mm	k_{Bal}	$>> k_{Fs}$; k_{Ug}
Ballast matting	none		–
Slab	t = 660 mm	k_{Ug}	72 and 52
Entire system		k	$1/(1/k_{Fs} + 1/k_{Ug})$ = 32.7 and 27.8

The analytical approach assuming load distribution in the longitudinal direction leads to plausible results: the obtained maximum bending moments are identical (as is ρ; see 2.1) in the two tests with flexural failure (Fig. 9a), although the measured shear forces at the supports are different between the two tests.

Furthermore, the assumed load distribution leads to different shear force lines in the testing areas compared to tests without superstructure (Fig. 9a+b). In Fig. 9b, it can be seen that the shear forces measured in the tests in which shear failure occurred were lower in the region without bent-up bars (1.0 m < x < 1.8 m). At x = 1.20 m, the calculated shear forces are identical in both tests with shear failure (Fig. 9b).

3.2. Comparison with tests on slab strips

In addition to the generally acknowledged size effect in shear failures, it is possible that the member width and load configuration could have a non-negligible effect on the shear capacity of one-way slabs without any shear reinforcement. In some studies, a possible positive effect of the member width on the shear capacity has been reported [24–26] while none was found in other publications [27–29]. Cantone et al. [30] recently analysed several results from the literature and concluded that the width likely has a favourable effect on the shear capacity for slabs with intermediate width-to-depth ratios ($1 < b/d < 5$). The favourable effect is explained by the variation in the shape and development of the critical shear crack, which allows the load to be redistributed. For larger width-to-depth ratios, these positive load redistribution effects may be counteracted by force concentrations leading to uneven force distribution, whether at load introduction points or due to the slab curvature at the bearings [30]. As the width-to-depth ratio in the conducted slab tests was 6.3, the shear resistances of the slabs that failed in shear should be similar to those of the preliminary tests on slab strips (width-to-depth ratio of 0.67). It should be noted that these considerations only apply to tests with strip loads and line supports.

The shear resistance of slabs can also be influenced by concentrated loads, as investigated in the presented tests. This topic has been investigated in several studies with tests on slabs [31–34] and on slabs under concentrated loads close to the support [35–37]. Many of the studies address the common concept of effective shear width in shear design (Fig. 1). This concept assumes a certain angle of distribution which is used to calculate the effective width for shear distribution [38]. As the slab specimens in the present study are designed with b/d = 6.3, the effective shear width concept suggests that more than 50% of the slab width has to be considered at a distance of 0.5d from the edge of the loading plate (see Fig. 10c). It should be noted that the spreading rule of

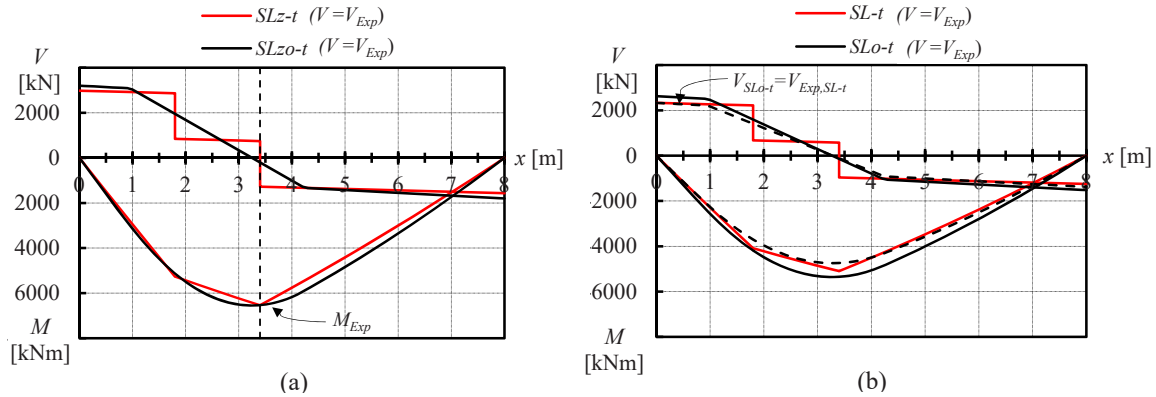

Fig. 9. Calculated stress resultants at load V_{Exp}: (a) tests with two rows of bent-up bars and (b) tests with a single row of bent-up bars.

[38] works only for the design of cantilevers with a single concentrated load. To consider the interaction of several loads and other static systems, finite-element analysis is required. Natário et al. [36] propose an approach in which the average unitary shear force over a distance of 4*d* is calculated based on linear–elastic finite-element models, using a reduced shear modulus and assuming a reduced Poisson's ratio to account for cracking. Reducing the elastic shear modulus by a factor of 8 and assuming the Poisson's ratio to be zero as suggested in [36] yields $v_{Exp} = 583.0$ kN/m for specimen SL–t at a distance of 0.5*d* from the edge of the loading plate. The average unitary shear force over the entire width is $v_{Exp} = 590.4$ kN/m. As both values are approximately the same, an influence on the shear capacity by concentrated loads can be neglected in this study.

The slab strip with two rows of bent-up bars (SSz–t) also exhibited flexural failure. The observed cracking pattern is similar to that observed in the corresponding slab test (SLz–t). The unitary bending capacity M_R at yielding (assuming mean values of the material properties listed in Tables 1 and 2 and a parabolic–rectangular stress distribution in the compression zone according to EC2 [39]) was almost the same in both tests (M_R = 1.59 MNm/m for SLz–t and 1.54 MNm/m for SSz–t). The comparison of these values with the maximum bending moments M_{Exp} determined from the experiment (formulas in Appendix A) shows that the bending capacity was slightly exceeded in both tests.

The slab strip with only one row of bent-up bars (SS–t) was loaded until the longitudinal reinforcing bars started to yield (at $V_{F,max}$ = 254.8 kN). After the load–deformation curve had flattened out, the specimen was unloaded slightly (–50 kN; see Fig. 10a). However, the subsequent re-loading step induced shear failure at $V_F = 231.0$ kN, a significantly lower load (–9.3%) than in the first loading branch (see Table 1). It is important to note that the shear crack opened vertically during unloading rather than decreasing or staying the same (Fig. 10d) that indicates that the point load stabilised the shear crack beforehand by supporting a direct strut. At the same time, the horizontal crack displacement stayed almost constant. In the re-loading stage, the horizontal and vertical displacements remained almost constant. In [16], the authors analysed specimen SS–t by evaluating shear-transfer actions based on measured surface deformations (as has been done in [40–42]). The result of this analysis showed that when the highest shear force $V_{F,max}$ acted, nearly the entire shear force must have been carried by compression strut action. The assumption of shear transfer by a direct struts can further be supported by a) pronounced delamination cracks along the longitudinal reinforcement and b) stable growth of crack displacements, even at very large crack widths (> 3 mm). As redistribution of forces must have taken place, the overall capacity is then defined by the capacities of the individual struts rather by the interaction of several shear transfer mechanisms at a flexural shear crack. However, a further increase in load was prevented either by the longitudinal reinforcement reaching its capacity or by the shear capacity after re-loading being exceeded. The shear capacity was lower in the re-loading step, presumably due to the changed kinematics. The crack pattern observed at the end of the test looks very similar to that of the corresponding slab test (SL–t, Fig. 10d). The critical shear crack originated in the region of the missing second row of bent-up bars and propagated almost horizontally to the second load introduction point. However, the slab strip exhibited higher normalised shear capacity (Fig. 10b). In the slab test, the above described force redistribution to direct struts is limited as the load is not introduced over the entire width and thus cannot support such struts in the same manner. As a consequence, the shear capacity of the slab was lower as it was defined by a combination of various shear transfer mechanisms in a flexural shear crack. The explanation given is supported as the observed capacity agrees well with the predictions of several models for the shear resistance of members without transverse reinforcement (Section 4).

In another test with a single point load at a distance $a = 3d$ from the support (SS, see Table 1), a 14% higher shear force acted ($V_{F,max}$ = 295.8 kN) before the specimen failed. The capacity of the compression zone near the load introduction point was reached and brittle crushing occurred.

As for the influence of the type of load introduction, direct strut action was found to be responsible for the higher capacity of the slab strip. In contrast, direct strutting is prevented if the load is not introduced over the entire width.

4. Analytical verification of the test results

4.1. Eurocode 2

Eurocode 2 (EC2) [39] stipulates that 50% of the transverse

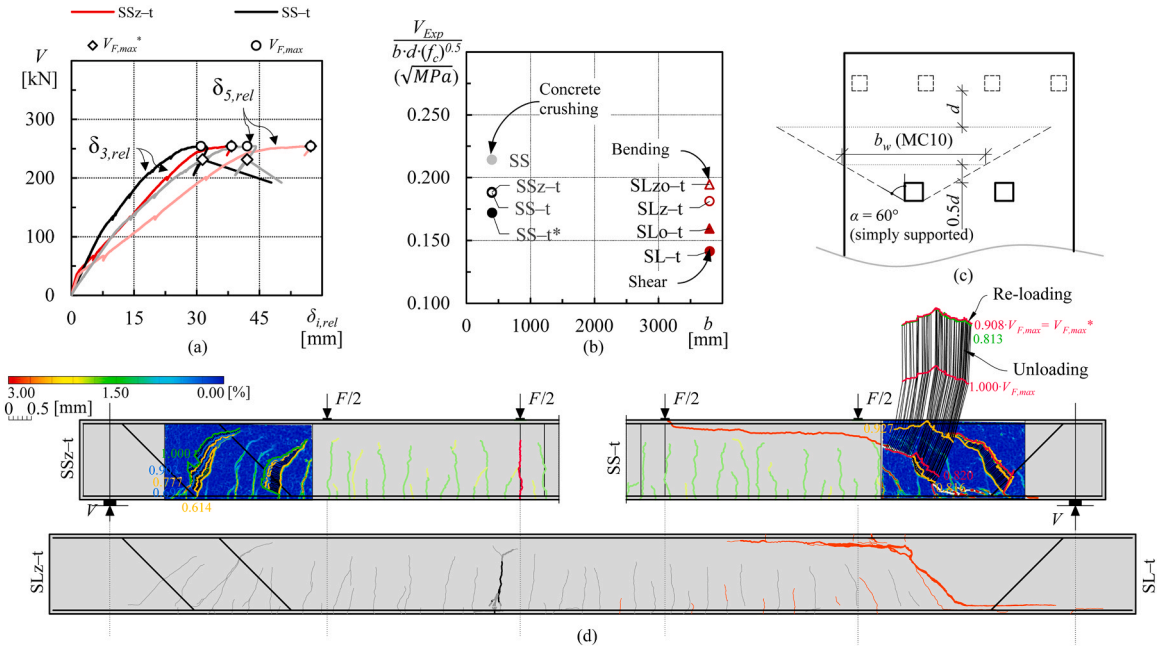

Fig. 10. Comparison between slab tests and slab strip tests: (a) effective widths for shear under concentrated loads [38]; (b) load–deflection curves; (c) comparison of the normalised shear capacity (d) comparison of crack patterns and observed kinematics in slab strips.

reinforcement in beams should consist of stirrups to transfer lateral forces. In slabs, these lateral forces can be transferred by transverse bars. According to EC2, the shear reinforcement can therefore consist entirely of bent-up bars ($\alpha \geq 30°$) if the force transferred by the compression strut does not exceed one-third of its capacity ($V_{Rd,max}$ in Eq. (4)). In EC2, the design of members with shear reinforcement is based on a truss model with variable concrete strut inclination (V_{Rd} in Eq. (4)) with a minimum capacity equal to the resistance provided by concrete ($V_{Rd,c}$ in Eq. (4)). There is no separate model for bent-up bars. In EC2, the maximum allowed distance between bent-up bars in a truss model is limited to $s_{b,max} < d$ in slabs and $s_{b,max} = 0.6{\cdot}d{\cdot}(1+\cot\alpha)$ in beams.

$$V_{Ed} \leq \max\{V_{Rd,c}; V_{Rd}\}, \text{ where}$$

$$V_{Rd} = \min\left\{\begin{array}{c} V_{Rd,s} = \frac{A_{sw}}{s} z{\cdot}f_{ywd}{\cdot}(\cot\theta + \cot\alpha){\cdot}\sin\alpha \\ V_{Rd,\max} = \alpha_{cw} b_w z \nu f_{cd}{\cdot}(\cot\theta + \cot\alpha)/\left(1+\cot^2\theta\right) \end{array}\right\} \quad (4)$$

and $V_{Rd,c}$ is the design value of the shear resistance for members not requiring shear reinforcement (see Appendix B), $V_{Rd,s}$ is the shear capacity of the tension ties, A_{sw} is the cross-sectional area of the shear reinforcement, s is the spacing of the shear reinforcement, z is the inner lever arm, f_{ywd} is the design yield strength of the shear reinforcement, θ is the angle between the concrete compression strut and the beam axis perpendicular to the shear force, α_{cw} is a coefficient taking into account the state of stress in the compression chord, b_w is the minimum width of the cross section, ν is the strength reduction factor for concrete cracked in shear and f_{cd} is the design value of the compressive cylinder strength of concrete.

4.2. fib Model Code 2010 and CSA

The fib Model Code 2010 (MC10) [38] provides three levels of approximation (LoA) for shear design with transverse reinforcement. In levels I and II, the contribution of the concrete is neglected. The level I approximation represents a variable angle truss model approach (as described in Section 4.1), while the level II approximation is based on a generalised stress field. The third level is based on the modified compression field theory (MCFT) [43], allowing a superposition of the contributions of concrete and reinforcement as a function of the longitudinal strain ε_x at half of the effective shear depth (Eq. (5)).

$$V_{Rd} = \min\left\{\begin{array}{c} V_{Rd,c} + V_{Rd,s} \\ V_{Rd,\max} = k_c f_{cd} b_w z/(\cot\theta + \tan\theta) \end{array}\right\}, \quad (5)$$

where k_c is a strength reduction factor taking into account the state of strain in the webs and the more brittle failure behaviour of higher-strength concretes, and θ is the inclination of the compressive stress field.

Similar rules are prescribed in the general method of the Canadian Code (CSA) [44]. Both fib Model Code 2010 and CSA accept bent-up bars with an angle of 30° or greater as shear reinforcement, provided that the inclined portion crossing potential diagonal cracks [38]. While the detailing of bent-up bars in one-way members is not addressed in MC10, the CSA states that "bent-up bars shall be spaced so that every 35° line, extending $d/2$ toward the reaction from mid-depth of member to longitudinal tension reinforcement, shall be crossed by at least one line of shear reinforcement". Moreover, only the centre three-quarters of the inclined portion of these bars may be considered effective.

4.3. ACI 318–19

In ACI318 [45,46], the design of shear reinforcement is based on a modified truss analogy, but, in contrast to EC2, the shear reinforcement needs to be designed to resist only the portion of the shear exceeding the limit at which inclined cracking occurs, provided the diagonal members in the truss are assumed to be inclined at 45° (Eq. (6)). The concrete is assumed to contribute to the shear capacity through resistance across the concrete compressive zone, aggregate interlock and dowel action in an amount equivalent to that which causes inclined cracking. ACI318 [45] considers bent-up bars as shear reinforcement which provide shear resistance due to having an inclined portion inclined at 30° or more with respect to the longitudinal bars and crossing potential diagonal cracks. Contrary to EC2 and MC10, the evaluation of a single group of parallel bars, as well as combinations with other types of shear reinforcement, is addressed explicitly (see Eq. (6)).

$$V_s \geq \frac{V_u}{\phi} - V_c, \text{ with}$$

$$V_s = \min\left\{\begin{array}{c} A_v{\cdot}f_y{\cdot}\sin\alpha \\ 3\sqrt{f_c'}\, b_w d \end{array}\right\} \text{for a single group of parallel bars, and}$$

$$V_s = \frac{A_v{\cdot}f_y{\cdot}(\sin\alpha + \cos\alpha){\cdot}d}{s} \text{for a series of groups of parallel bars,} \quad (6)$$

where A_v is the cross-sectional area of the shear reinforcement, f_c' is the specified compressive strength of concrete, V_u is the factored shear force at the relevant section and ϕ is the strength reduction factor (for shear: 0.75).

ACI states that "longitudinal bars bent to act as shear reinforcement shall be spaced so that every 45° line, extending $d/2$ toward the reaction from mid-depth of member to longitudinal tension reinforcement, shall be crossed by at least one line of shear reinforcement." Further, shear reinforcement may consist of only bent-up bars. Enclosing of compression reinforcement for beams is required in order to prevent buckling of the reinforcing bars.

4.4. ÖN B4008-2

In the only recent systematic studies on bent-up bars [16,48], various configurations of bent-up bars were tested. The results confirmed that the spacing limits stipulated in EC2 (Section 4.1) are suitable to foster the development of a truss system of tension ties and compression struts. Tested members with wide spacings between bent-up bars ($> d$) showed that crack propagation and the associated cracking patterns were similar to those in beams without shear reinforcement. Thus, a well-pronounced rotating crack formed instead of smeared and more inclined cracks. The tests were analysed by evaluating shear transfer actions with the help of photogrammetric measurements. It became evident that shear transfer actions assigned to the concrete (aggregate interlock, fracture process zone, inclined strut in the uncracked compression zone) and those assigned to the reinforcement (tensile action and dowel action) act together in such cases. Based on these findings, a semi-empirical model with a mechanical basis (potential shear crack model; PSCM) for advanced structural assessment of bridges with widely spaced bent-up bars was formulated [3,47]. This model was integrated in the Austrian standard ÖN B4008–2 (B4008) [17] to assess the load capacity of existing bridge structures.

According to ÖN B4008–2, the contribution of the concrete to the shear strength V_c can be simply described as a reduced value of the pure shear resistance of the concrete V_{c0} multiplied by the coefficient k_i (Eq. (7)) which is dependent on the ratio of the individual contributions of concrete and steel (V_s/V_{c0}). The total shear resistance V_R considering bent-up bars can be calculated as follows (Eq. (7)):

$$V_R = V_s + V_{c0}\cdot k_i \text{ and}$$
$$V_s = V_{bu} + V_{sw} = \sum A_{bu}\cdot f_{yb}\cdot \sin\alpha + \sum A_{sw}\cdot f_{yw},$$
$$V_{c0} = \kappa\cdot\left(100\cdot\rho\cdot f_{ck}\frac{d_{dg}}{\sqrt{a\cdot d/4}}\right)^{1/3}\cdot b_w d \ \text{[N]}, \quad (7)$$
$$k_i = 1 - 0.125\cdot V_s/V_{c0} \geq 0.0$$

where V_{c0} is the shear strength of concrete according to [49,50], $\kappa = 0.6$ is a calibration factor, d_{dg} ($= 16+d_g \leq 40$ mm if $f_{ck}<60$ MPa) is a size parameter describing the failure zone roughness, d_g is the maximum aggregate size and $a = M/V$ is the shear span. For moving loads, which are common in infrastructure structures, the root in the denominator can be replaced by d.

The formulations are rather similar to the concept developed by Thürlimann [51] which was used in the CEB-FIP Model Code 1978 [52] for the more refined verification of the shear resistance. The load-bearing portion of the concrete is reduced in a similar fashion, by considering the acting shear force.

4.5. Comparison and structural analysis

The rules of the standards described in Sections 4.1 to 4.4 are compared and applied to verify the shear resistance observed in the tests presented in Section 2. Fig. 11 shows the comparison of maximum spacings of bent-up bars of several standards (dashed grey lines) with the actual spacings of the test specimens. The maximum spacing determined with the approach described in ÖN B4008 (Section 4.4) ensures that at least one group of parallel bent-up bars is crossed by a potential shear crack (Fig. 11).

In EC2, MC10 and ACI318, detailing limits prevent the application of the truss model (Eqs. (4) and (6)) or stress field approaches (Eq. (5)). Even so, and to aid understanding, the resistances obtained from these models are depicted by coloured dashed lines in Fig. 11. In EC2 and MC10, only the contribution of the concrete $V_{Rd,c}$ is thus considered, as no other model is given in these documents. As the spacing between the rows of bent-up bars is rather large in the tests ($s_b = 1.33\cdot d$, Table 1), only the shear resistance for a single bent-up bar can be calculated according to ACI318 (Eq. (6)). A combination of steel and concrete contributions can be considered only when using ACI318 or B4008. Table 8 summarises the contributions that can be considered for beams or slabs. They are also visualised in Fig. 11 (coloured solid lines and grey hatchings in the shear force diagram).

Table 9 shows the detailed results of the analytical verification of the shear resistance according to various design standards. The results are compared with the acting shear force calculated according to Appendix B for specific sections (e.g., significant changes in the shear resistance curve in Fig. 11).

The verification results show that current design standards (EC2, MC10&CSA, ACI) tend to underestimate the shear strength of slabs designed with bent-up bars with wide spacings due to detailing rules. Thus, they are not adequate for the assessment of existing structures. Even if detailing limits for the application of the truss model according to EC2 are ignored, capacity reserves become apparent (Fig. 11a). It should be noted, however, that ignoring these limits in the ACI approach would lead to remarkably high resistances due to the superposition of the steel and concrete contributions (Fig. 11c). The reason lies in the possibility of using either of two formulas for the concrete contribution (see Appendix B). Only one of these takes into account the longitudinal reinforcement ratio, which is rather low at the support ($\rho = 0.44\%$, Fig. 3). The stress field approach found in MC10 (CSA) yields plausible results if spacing limits are ignored (Fig. 11b). The potential shear crack model introduced in ÖN B4008 is the only model which yields results similar to the test results. The shear resistance function displayed in Fig. 11d lies slightly above the acting shear forces determined in the tests with a second row of bent-up bars (SLz–t and SLzo–t). As the cracking

Table 8
Considered contributions to the shear capacity according to current standards for the analytical verification of the tests with bent-up bars (Table 1).

Component	*EC2*	*MC10 (CSA)*	*ACI318*	*B4008*
Beams	$V_{Rd,c}$ (stirrups <50% or single row)	$V_{Rd,c}$ ($s_b >$ 0.96·d)	V_S+V_C (V_s of a single bent-up bar, since $s_b >$ 0.71·d)	$V_S+V_{C0}\cdot k_i$
Slabs ($A_{s,secondary} \geq 0.2\cdot A_s$)	$V_{Rd,c}$ ($s_b > d$)			

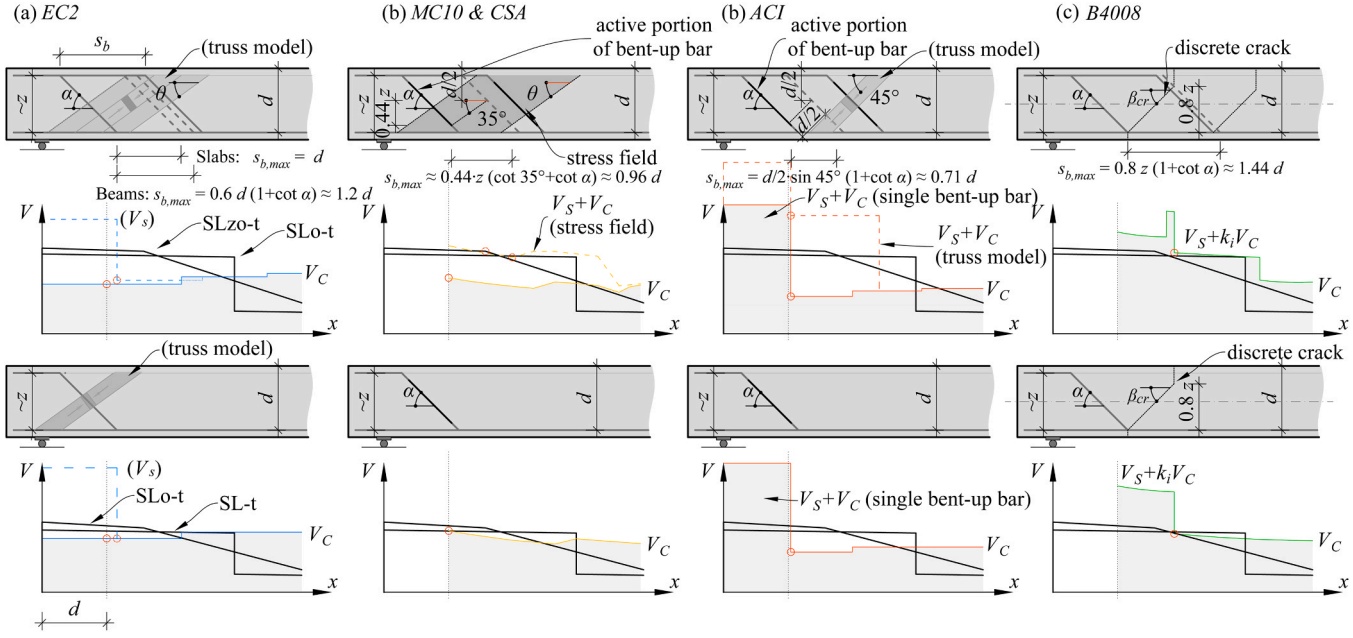

Fig. 11. Comparison of the analytical shear resistances obtained with approaches from various design standards (coloured solid lines) with those from the slab tests (black solid lines): (a) EC2; (b) MC10 (CSA); (c) ACI318; (d) ÖN B4008.

Table 9
Analytical verification of the shear resistance according to various standards.

Data		*EC2*				*MC10 (CSA)*				*ACI*				*B4008*			
Test		x (m)	V_E (kN)	V_R (kN)	V_E/V_R (–)	x (m)	V_E (kN)	V_R (kN)	V_E/V_R (–)	x (m)	V_E (kN)	V_R (kN)	V_E/V_R (–)	x (m)	V_E (kN)	V_R (kN)	V_E/V_R (–)
SL1	SLz–t	0.605	2943.2	1850.4	1.59	0.605	2943.2	2089.8	1.41	0.652	2940.1	1388.1	2.12	1.136	2909.6	3030.4	0.96
		0.700	2937.0	(1997.3)	(1.47)	1.2	2905.61	(2851.0)	(1.02)	0.652	2940.1	(4422.4)	(0.66)				
	SL–t	0.605	2291.8	2009.3	1.14	0.605	2291.8	2293.3	1.00	0.652	2288.7	1507.3	1.52	1.136	2257.3	2187.8	1.03
SL2	SLzo–t	0.605	3129.2	1850.4	1.69	0.605	3129.2	2089.8	1.50	0.652	3123.0	1388.1	2.25	1.136	2845.6	3030.4	0.94
		0.700	3116.8	(1997.3)	(1.56)	0.95	3085.9	(3009.3)	(1.03)								
	SLo–t	0.605	2551.8	2009.3	1.27	0.605	2551.8	2293.3	1.11	0.652	2545.6	1507.3	1.83	1.136	2299.4	2187.8	1.05

Values in brackets show resistances calculated for truss model and stress field approaches.

pattern in those tests showed pronounced shear cracking in this region (Fig. 7), the authors suggest that the shear capacity was almost reached. The shear capacity and failure location for the tests with only one row of bent-up bars were predicted quite well. These results also indicate that the approach for longitudinal load distribution described in Section 3.1 is valid, as the calculated shear force in the failure locations are almost the same as those predicted from the model.

5. Summary and conclusions

This investigation deals with the experimental and theoretical assessment of the shear capacity of slab bridges designed with bent-up bars. To span the knowledge gap between the load-bearing behaviour of small-size specimens and actual structures, the results of four shear tests on two full-scale replica slabs under realistic loading conditions are presented. Based on the findings of this analysis, the following conclusions are drawn:

- The presence of a complete track superstructure showed an evident load distributing effect in the longitudinal direction. To take this into account, the model proposed by Zimmermann based on a beam on elastic foundation, is considered adequate. This approach leads to plausible results and confirms the rules for load distribution given in Eurocode 2. The application of such a refined model may lead to an advantageous shear force line if the superstructure consists of several elastic layers.
- The comparison of the full-scale tests with preliminary tests on slab strips with a tenth of the width showed differences in the load-bearing behaviour of small-format laboratory tests. Direct struts between the applied force and the bends of the bent-up longitudinal bars or the bearings are likely to develop if loads are introduced over the whole width, which is typical for laboratory tests on slab strips. In real bridge structures, however, direct strutting is limited due to the introduction of point loads in wide members. This causes the shear capacity values of the slab strips to be greater than those of the slab specimens. Nevertheless, the experimentally obtained shear capacities of regions without shear reinforcement of the slabs were in sound agreement with the predictions of several standards and thus the models are considered adequate for cases when the load is not introduced over the entire width.
- The analytical verification of the test results according to several design standards shows the potential of the newly developed potential shear crack model for assessing the shear capacity of slab bridges with widely spaced bent-up bars. The approach of evaluating the shear resistance at several locations is a suitable way to consider bent-up bars with variable diameters and spacings. The detailing rules of current design standards (Eurocode 2, fib Model Code 2010, CSA A23.3-04, ACI 318-19), however, hinder the application of shear models for existing structures designed with bent-up bars with wide spacings, and thus the actual shear resistance of such structures is likely to be underestimated with these approaches. Thus, they are not adequate for the assessment of such structures.

Funding

This research was funded by ÖBB Infrastruktur AG, grant number PROVIA ID – 1924.

CRediT authorship contribution statement

Tobias Huber: Conceptualization, Formal analysis, Investigation, Methodology, Project administration, Software, Visualization, Writing – original draft, Writing – review & editing. **Johann Kollegger:** Supervision, Writing – review & editing. **Patrick Huber:** Conceptualization, Funding acquisition, Investigation, Methodology, Project administration, Supervision, Writing – review & editing. **Markus Vill:** Funding

acquisition, Project administration, Writing – review & editing. **Hannes Wolfger:** Investigation, Writing – review & editing.

Declaration of Competing Interest

The authors declare the following financial interests/personal relationships which may be considered as potential competing interests: Tobias Huber reports financial support was provided by ÖBB-Infrastruktur AG.

Data availability

Data will be made available on request.

Acknowledgements

The authors acknowledge the financial support by TU Wien Bibliothek through its Open Access Funding Programme. Furthermore, thank is given to ÖBB for providing the testing site. The authors would also like to thank all parties involved for the successful cooperation.

Appendix A. Calculation of stress resultants

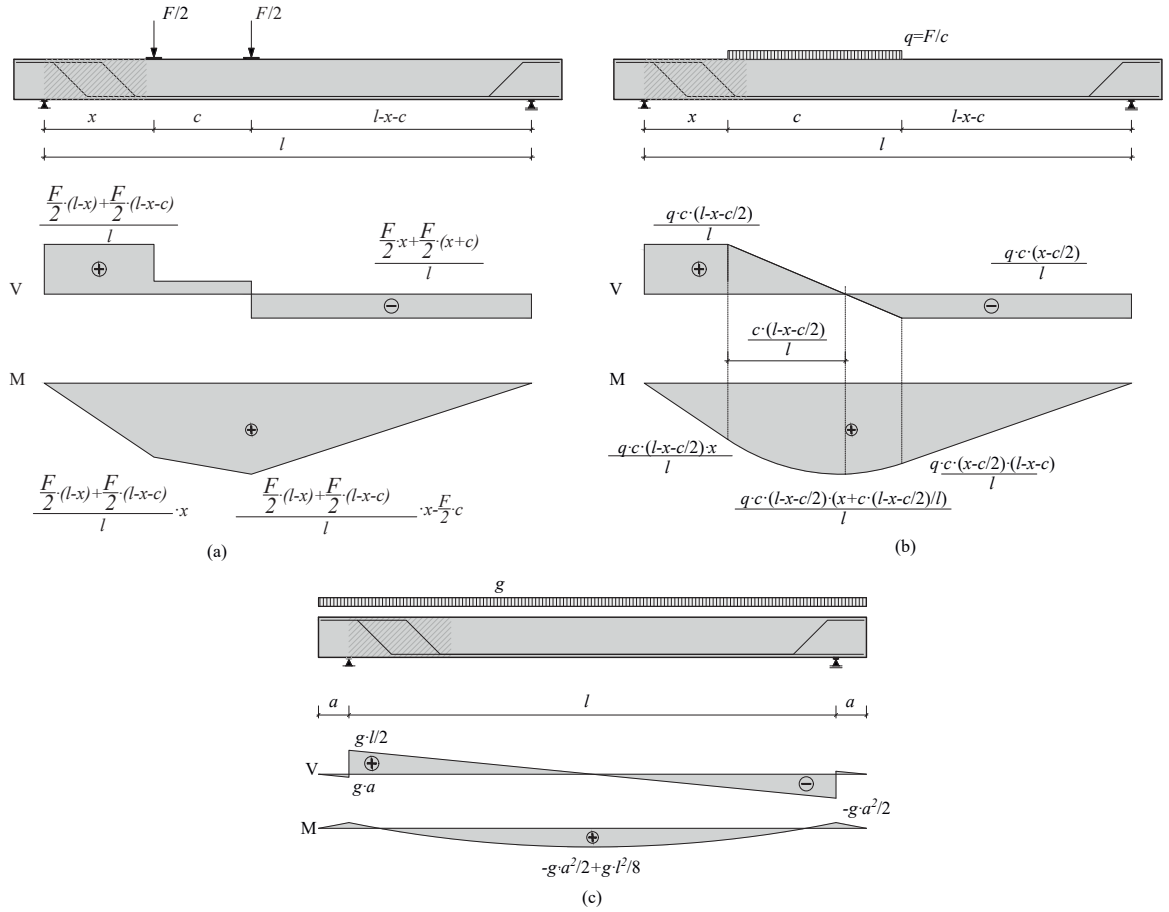

Figure 12. Calculation of stress resultants for (a) direct loading, (b) load distribution by superstructure and (c) dead load.

Appendix B. Shear provisions for structures without shear reinforcement according to several standards

Eurocode 2 [39]:

$$V_{Rd,c} = \max\left\{ \begin{array}{c} \left[\frac{C_{R,c}}{\gamma_c} k (100 \rho f_{ck})^{1/3} + k_1 \sigma_{cp}\right] b_w d \\ (0.035 k^{3/2} f_{ck}^{1/2} + k_1 \sigma_{cp}) b_w d \end{array} \right\}$$

***fib* Model Code 2010** [38]:

$$V_{Rd,c} = k_v \frac{\sqrt{f_{ck}}}{\gamma_c} z b_w ; \sqrt{f_{ck}} \leq 8 MPa$$

– LoA I

C_{Rc}… Calibration factor (recommended value: 0.18 [39])
γ_c… Partial safety factor for concrete (=1.5 [39])
$k = 1 + (200/d\ [\text{mm}])^{0,5}$… Size factor
$\rho \leq 0.02$… Longitudinal reinforcement ratio
f_{ck}… Characteristic value of the concrete cylinder compressive strength
k_1… Factor for normal stresses (=0.15 [39])
$\sigma_{cp} < 0.2 \cdot f_{cd}$… Normal stress (positive for compression)
b_w… Minimum width of the cross section
d… Static depth
z… Inner lever arm
$k_{dg} = 32/(16 + d_g) \geq 0.75$
d_g… Maximum size of aggregate
ε_x… Strain at half of the effective shear depth
M_{Ed}, V_{Ed}, N_{Ed}…Stress resultants

(*continued on next page*)

(*continued*)

$k_v = \frac{180}{1000 + 1.25 \cdot z\ (\text{mm})}$ – LoA II $k_v = \frac{0.4}{1 + 1500\varepsilon_x} \frac{1300}{1000 + k_{dg} \cdot z\ (\text{mm})}$ $\varepsilon_x = \frac{\left(\frac{M_{Ed}}{z} + V_{Ed} + N_{Ed}\frac{z_p - e_p}{z}\right)}{2\left(\frac{z_s}{z}E_s A_s + \frac{z_p}{z}E_p A_p\right)}$; $0 \le \varepsilon_x \le 0{,}003$ $\varepsilon_s \le \frac{\varepsilon_{sy}}{2}$	E… Young's modulus A… Cross-sectional area of the bars $_s$… Reinforcing bars $_p$… Tendons
ACI 318–19 [45]: $A_{v,\,\min}/s = \max\left\{0.75\sqrt{f_c'}\ \frac{b_w}{f_{yt}}; 50\frac{b_w}{f_{yt}}\right\}$ for non-prestressed beams. For $A_v \ge A_{v,min}$: V_c = eitherof $\left\{\begin{array}{c}\left[2\lambda\sqrt{f_c'} + \frac{N_u}{6 \cdot A_g}\right] b_w d \\ \left[8\lambda_s \lambda (\rho_w)^{1/3}\sqrt{f_c'} + \frac{N_u}{6 \cdot A_g}\right] b_w d\end{array}\right\}$ For $A_v < A_{v,min}$: $V_c = \left[8\lambda_s \lambda (\rho_w)^{1/3}\sqrt{f_c'} + \frac{N_u}{6 \cdot A_g}\right] b_w d$ $V_c \le 5\lambda\sqrt{f_c'} b_w d$ and $\frac{N_u}{6 \cdot A_g} \le 0.05 f_c'$ $\lambda_s = \sqrt{\frac{2}{1 + d/10}} \le 1$, $\sqrt{f_c'} \le 100\text{psi}$	N_u… Axial load (positive for compression) A_g… Gross area of concrete section f_c'… Specified compressive strength of concrete λ… Modification factor for lightweight concrete relative to normal-weight concrete of the same compressive strength ρ_w… ratio of A_s to $b_w \cdot d$

References

[1] Fischer O, Müller A, Lechner T, Wild M, Kessner K. Findings and insights concerning the results of re-analyzed concrete bridges in Germany. Beton und Stahlbetonbau 2015;2:107–27. 109.

[2] Fédération Internationale du Béton (fib). Towards a rational understanding of shear in beams and slabs (workshop proceedings). Fib Bull 2018;85:1–338.

[3] Huber T, Huber P, Kollegger J. Shear strength model for existing RC components with bent-up bars (in German). Beton und Stahlbetonbau 2020;10:811–20. 115.

[4] Leonhardt F, Walther R. Schubversuche an Plattenbalken mit unterschiedlicher Schubbewehrung. Deutscher Ausschuss für Stahlbeton, 156. Berlin: Ernst & Sohn,; 1963. p. 1–84.

[5] Mörsch, E. (1908). Der Eisenbetonbau, seine Theorie und Anwendung. Stuttgart: K. Wittwer Verlag.

[6] Deutscher Ausschuß für Stahlbeton (1973). DIN 1045-Teil A: Bestimmungen für Ausführung von Bauwerken aus Stahlbeton. Berlin: Deutscher Ausschuß für Stahlbeton,

[7] ÖNORM B4200–4. Stahlbetontragwerke – Berechnung und Ausführung. Vienna: Austrian Standards Institute; 1957.

[8] Huber P, Schweighofer A, Kollegger J, Brunner H, Karigl W. Comparison of the calculative shear resistance of existing bridges according to Eurocode 2 and fib Model Code 2010. Beton Stahlbetonbau 2012;7:451–62. 107.

[9] Schacht G, Müller L, Curbach M, Marx S. Shear bearing behaviour of reinforced concrete slabs for building constructions. Beton- und Stahlbetonbau 2013;9: 592–602. 108.

[10] Deutscher Ausschuß für Stahlbeton (1972). DIN 1045: Beton- und Stahlbetonbau – Bemessung und Ausführung. Berlin: Deutscher Ausschuß für Stahlbeton.

[11] Austrian Standards Institute. ÖNORM B4200–8: Stahlbetontragwerke – Berechnung und Ausführung. Vienna: Austrian Standards Institute,; 1969.

[12] Özden, K. (1967). An Experimental Investigation on the Shear Strength of Reinforced Concrete Beams: Tests Performed at Structural Research Laboratory, Technical University of Denmark. Technical University of Istanbul Faculty of Civil Engineering: Istanbul, 1–243.

[13] Leksukhum K, Smith R. Comparative Study of Bent-up Bars with other Forms of Secondary Reinforcement in Beams, 68.1. ACI Special Publication,; 1971. p. 32–5.

[14] Regan P, Khan M. Bent-Up Bars as Shear Reinforcement, 42. ACI,; 1974. p. 249–66.

[15] Bagge N, Popescu C, Elfgren L. Failure tests on concrete bridges: Have we learnt the lessons? Struct Infrastruct Eng 2018;14-3:292–319.

[16] Huber T, Huber P, Fasching S, Vill M, Kollegger J. Shear behavior of RC components with bent-up bars based on photogrammetric measurements. Bauingenieur 2020;95-6:181–93.

[17] Austrian Standards International. ÖN B 4008–2: Assessment of load capacity of existing structures – Part 2: Bridge construction. Vienna: Austrian Standards International,; 2019.

[18] Vospernig M, Reiterer M. Evaluation of the dynamic system characteristics for single span concrete railway bridges – Determination of dynamic parameters due to measurements on two test bridges in cracked and uncracked state with variations of the dead load. Beton-und Stahlbetonbau,; 2020115–6424–437.

[19] CEN. EN 1991–2: Eurocode 1: Actions on structures – Part 2: Traffic loads on bridges. Brussels: Comité Européen de Normalisation,; 2003.

[20] Winkler, E. (1867). Die Lehre von der Elasticitaet und Festigkeit: mit besonderer Rücksicht auf ihre Anwendung in der Technik, für polytechnische Schulen, Bauakademien, Ingenieure, Maschinenbauer, Architecten, etc. Prague: H. Dominicus.

[21] Zimmermann H. Die Berechnung des Eisenbahnoberbaues. Berlin: Ernst & Sohn,; 1941.

[22] Köhler, M. (2002). Der Bettungsmodul für den Schotteroberbau von Meterspurbahnen. Doctoral thesis, Eidgenössische Technische Hochschule Zürich.

[23] Kuttelwascher, C., & Zuzic, M. (2013). Oberbauschotter-Kompendium für Österreich. Eisenbahn Ingenieur Kalender EIK, 100–126.

[24] Conforti A, Minelli F, Plizzari GA. Influence of width-to-effective depth ratio on shear strength of reinforced concrete elements without web reinforcement. Acids Struct J 2017;114(4):995.

[25] Leonhardt F, Walther R. The Stuttgart Shear Tests. Beton- und Stahlbetonbau 1962; 8(1962):1962. 57.

[26] De Cossio, D. R. Joint ACI-ASCE Committee 326 discussion of shear and diagonal tension. ACI J Proc, 59; 1962. p. 1323–32. Jan. 1962.

[27] Adam V, Herbrand M, Classen M. Experimental investigations on the influence of the slab width and the moment-shear-ratio on the shear capacity of RC slabs without shear reinforcement. Bauingenieur 2018;93(1):37–45.

[28] Kani GNJ. How safe are our large reinforced concrete beams? Acids J Proc 1967;V. 64(No. 3):128–41. Mar. 1967.

[29] Regan, P.E. (1982). Tests of the Wide-beam Shear Resistance of Concrete Slabs. Structures Research Group, Polytechnic of Central London, London, UK, Apr. 1982.

[30] Cantone R, Fernández Ruiz M, Muttoni A. Shear force redistributions and resistance of slabs and wide beams. Struct Concr 2021;22(4):2443–65.

[31] Reissen K, Classen M, Hegger J. Shear in reinforced concrete slabs—experimental investigations in the effective shear width of one-way slabs under concentrated loads and with different degrees of rotational restraint. Struct Concr 2018;19(1): 36–48.

[32] Sherwood EG, Lubell AS, Bentz EC, Collins MP. One-way shear strength of thick slabs and wide beams. Acids Struct J 2006;103(6):794.

[33] Regan PE, Rezai-Jorabi H. Shear resistance of one-way slabs under concentrated loads. Struct J 1988;85(2):150–7.

[34] Rodrigues RV, Ruiz MF, Muttoni A. Shear strength of R/C bridge cantilever slabs. Eng Struct 2008;30(11):3024–33.

[35] Lantsoght EO, van der Veen C, Walraven JC. Shear in one-way slabs under concentrated load close to support. Acids Struct J 2013;110(2):275.

[36] Natário F, Ruiz MF, Muttoni A. Shear strength of RC slabs under concentrated loads near clamped linear supports. Eng Struct 2014;76:10–23.

[37] Regan PE. Shear resistance of concrete slabs at concentrated loads close to supports. London, UK: Polytechnic of Central London; 1982. p. 1–24.

[38] fib – Fédération Internationale du Béton. Fib model code for concrete structures 2010. Berlin: Ernst & Sohn; 2013.

[39] CEN. EN1992-1-1 Eurocode 2 design of concrete structures – Part 1-1: general rules and rules for buildings. Brussels: Comité Européen de Normalisation; 2005.

[40] Huber P, Huber T, Kollegger J. Investigation of the shear behavior of RC beams on the basis of measured crack kinematics. Eng Struct 2016;113:41–58.

[41] Campana S, Fernandez Ruiz M, Anastasi A, Muttoni A. Analysis of shear-transfer actions on one-way RC members based on measured cracking pattern and failure kinematics. Mag Concr Res 2013;65(5-6):386–404.

[42] Cavagnis F, Ruiz MF, Muttoni A. An analysis of the shear-transfer actions in reinforced concrete members without transverse reinforcement based on refined experimental measurements. Struct Concr 2018;19(1):49–64.

[43] Bentz EC, Vecchio FJ, Collins MP. Simplified modified compression field theory for calculating shear strength of reinforced concrete elements. Acids Struct J 2006;103 (4):614–24.
[44] CSA (Canadian Standards Association) Committee A23.3. Design of concrete structures. Toronto, ON, Canada: CSA Group; 2004. p. 240.
[45] ACI (American Concrete Institute). ACI 318-19: building code requirements for structural concrete and commentary. Farmington Hills, MI, USA: American Concrete Institute,; 2019.
[46] Kuchma DA, Wei S, Sanders DH, Belarbi A, Novak LC. Development of the one-way shear design provisions of ACI 318-19 for reinforced concrete. Acids Struct J 2019; 116(4):285–96.
[47] Huber T, Untermarzoner F, Kollegger J. Experimental investigation and mechanical modelling of shear failure in reinforced concrete members with plain and ribbed bent-up bars. Eng Struct 2023;283:115793.
[48] Huber, T. (2019). Assessment of the shear resistance of existing reinforced concrete bridges with bent-up bars (in German) (Doctoral thesis), TU Wien,
[49] Cavagnis F, Ruiz MF, Muttoni A. A mechanical model for failures in shear of members without transverse reinforcement based on development of a critical shear crack. Eng Struct 2018;157:300–15.
[50] CEN. FprEN 1992-1-1: Eurocode 2 – design of concrete structures – Part 1-1: general rules and rules for buildings, bridges and civil engineering structures. Brussels: Comité Européen de Normalisation; 2023.
[51] Thürlimann, B.1978. Shear strength of reinforced and prestressed concrete beams. In: CEB Bulletin D'Information 126. p. 16–38.
[52] CEB-FIP1978. Model Code for Concrete Structures 1978. Lausanne: Comité Euro-International du Béton (CEB).